Hindawi
International Journal of Aerospace Engineering
Volume 2017, Article ID 4326018, 10 pages
https://doi.org/10.1155/2017/4326018

Research Article

Ionospheric Gradient Threat Mitigation in Future Dual Frequency GBAS

Michael Felux,[1] Mihaela-Simona Circiu,[1] Jiyun Lee,[2] and Florian Holzapfel[3]

[1]*German Aerospace Center (DLR), Münchener Straße 20, 82234 Weßling, Germany*
[2]*Korea Advanced Institute of Science and Technology (KAIST), 291 Daehak-ro, Yuseong-gu, Daejeon 34141, Republic of Korea*
[3]*Institute of Flight System Dynamics, Technische Universität München (TUM), Boltzmannstraße 15, 85748 Garching, Germany*

Correspondence should be addressed to Michael Felux; michael.felux@dlr.de

Received 15 December 2016; Revised 15 February 2017; Accepted 27 February 2017; Published 20 March 2017

Academic Editor: Antonio Angrisano

The Ground Based Augmentation System (GBAS) is a landing system for aircraft based on differential corrections for the signals of Global Navigation Satellite Systems (GNSS), such as GPS or Galileo. The main impact on the availability of current single frequency systems results from the necessary protection against ionospheric gradients. With the introduction of Galileo and the latest generation of GPS satellites, a second frequency is available for aeronautical navigation. Dual frequency methods allow forming of ionospheric free combinations of the signals, eliminating a large part of the ionospheric threats to GBAS. However, the combination of several signals increases the noise in the position solution and in the calculation of error bounds. We, therefore, developed a method to base positioning algorithms on single frequency measurements and use the second frequency only for monitoring purposes. In this paper, we describe a detailed derivation of the monitoring scheme and discuss its implications for the use in an aviation context.

1. Introduction

In modern aviation, the navigation methods are increasingly based on the use of Global Navigation Satellite Systems (GNSS). This transition away from conventional terrestrial navigation aids enables a more efficient use of the airspace and provides a seamless global navigation capability. A key aspect of using GNSS is the provision of integrity, that is, a high level of trust an airborne user can put into the position solution. For different phases of flight different methods and augmentation systems can be used to achieve different levels of integrity. Receiver autonomous integrity monitoring (RAIM) is based on consistency checking of redundant GNSS measurements and is used today in support of RNP (Required Navigation Performance) operations. Advanced RAIM (ARAIM) using multiple GNSS constellations with a light integrity support will provide horizontal services soon and vertical guidance at a later stage [1]. Space based augmentation systems (SBAS) are certified for use also for precision approaches (with a certain minimum visibility still required) [2]. GBAS is currently certified for CAT I operations (or GBAS Approach Service Type (GAST) C in GBAS terminology) and is operational and in regular use at a number of locations around the world including Bremen and Frankfurt in Germany, Newark and Houston in the US, Sydney in Australia, Zurich in Switzerland, and Malaga in Spain. The standards for GBAS supporting CAT II/III operations (i.e., with lower or no limitations regarding minimum visibility, termed as GAST D in the GBAS community), were agreed upon by the International Civil Aviation Organization (ICAO) at the end of 2016. First stations supporting this new service type could become operational as soon as 2018. In GBAS a ground station with four (or potentially more) reference receivers at carefully surveyed sites at an airport generates corrections for the GNSS signals and broadcasts them to arriving aircraft. Along with those corrections, a set of integrity parameters is broadcast to enable the aircraft to calculate error bounds for the differentially corrected positions. Stations designed for GAST C and GAST D, however, only rely on signals from the GPS constellation in the L1 frequency band. A significant

number of different monitors in the ground and airborne systems may result in limited availability due to frequent trips, especially in equatorial and auroral regions prone to high ionospheric activity.

A challenge for GNSS users is ionospheric scintillations. This effect leads to degraded signal tracking quality in the receiver or loss of lock to several satellites and thus results in degraded satellite geometries [3–5]. Use of signals from multiple GNSS constellations will provide significantly increased robustness against this kind of events due to the large number of satellites and thus low sensitivity to the loss of individual signals. A different threat for GBAS results from ionospheric gradients, that is, strong variations of electron density in the ionosphere over a short distance [6, 7]. This threat can be addressed by means of dual frequency positioning eliminating the ionospheric delay (to a first order which is sufficient for GBAS operations) in GNSS measurements. GPS introduced signals on a second frequency usable for safety of life applications with the latest generation of satellites (Block IIF). Galileo provides those signals on all its satellites from the beginning. Combining measurements from two frequencies, however, comes at the cost of significantly increasing the residual noise in the position solution due to the combination of the two noisy pseudorange measurements on L1/E1 and L5/E5a [8]. It is thus a likely scenario that even in future GBAS with dual frequency capability positioning in the nominal case will be based on single frequency measurements. In that case, an effective monitoring for ionospheric gradients is necessary. In this paper, we describe a method how this can be achieved and show results from testing this method in flight trials.

2. Generation of GBAS Corrections

In order to understand the difficulty of dual frequency ionospheric monitoring, we start by describing how the corrections are generated in a GBAS ground station according to [9]. In a first step, the pseudoranges $\rho(i, j)$, measured for satellite i at the reference receiver j, are passed through a low pass Hatch filter [10]. This process removes a large part of the noise and multipath errors. From the geometric range $R(i, j)$, the carrier smoothed code measurement $\rho_{\text{csc}}(i, j)$ and the correction for the satellite clock $c\Delta t_{\text{SV},j}$ are subtracted in order to obtain a preliminary candidate for a pseudorange correction $\text{PRC}_{\text{prel}}(i, j)$:

$$\text{PRC}_{\text{prel}}(i, j) = R(i, j) - \rho_{\text{csc}}(i, j) - c\Delta t_{\text{SV},j}. \quad (1)$$

The geometric range can be calculated due to precise knowledge of the reference antenna location and the known satellite position. The satellite clock correction is calculated based on parameters transmitted in the satellite navigation message. Repeating this process for each satellite in view yields a set of candidate corrections from one receiver. These correction candidates, however, all contain the receiver clock error. In order to remove the individual clock errors from the correction candidates of each receiver, a process called smooth clock adjustment is performed. In this step, the weighted average over all N correction candidates from one receiver is removed with the condition that the sum of all weights $\sum_{i=1}^{N} k_i = 1$.

$$\text{PRC}_{\text{sca}}(i, j) = \text{PRC}_{\text{prel}}(i, j) - \sum_{i=1}^{N} k_i \cdot \text{PRC}_{\text{prel}}(i, j). \quad (2)$$

This can be done without affecting the positioning since any bias common to all satellites only projects into the user clock estimate. It is important to note, however, that in this step all biases common to all satellites are removed. This is especially true for the part of the ionospheric delay that is common to all satellites. An illustration of this process is shown in Figure 1.

An estimation of the experienced ionospheric delay at the reference receiver by analyzing the corrections is therefore not possible anymore. After repeating this process for each reference receiver, the final correction to be transmitted to the user is the average of the smoothed and clock adjusted corrections from all $M(i)$ receivers that track the particular satellite i.

$$\text{PRC}_{tx}(i) = \frac{1}{M(i)} \sum_{j} \text{PRC}_{\text{sca},\tau}(i, j). \quad (3)$$

Additionally, a set of range rate corrections (RRC) is formed based on the pseudorange corrections. It is generated by dividing the difference of the PRC at the current epoch and the previous epoch by the time between the two epochs. This is done to allow the aircraft to interpolate between the reception of two sets of corrections.

In the current service types, C and D, the corrections are only formed for pseudorange measurements of GPS L1 C/A code measurements. Future processing modes will also provide corrections and integrity parameters for signals from other constellations as well as for signals on a second frequency (L5/E5a) [11, 12]. These corrections shall enable another single frequency mode based on L5 signals, should the L1 signal be unavailable, and also a dual frequency mode in order to enable ionosphere free positioning to address the ionospheric gradient threat. While the steps of forming the corrections are assumed to be the same also for the new signals, it is important to note that the smooth clock adjustment process described in (2) will result in very different averages for different frequencies. This is due to the fact that not necessarily the same set of satellites will be used (GPS satellites before Block IIF do not yet provide L5 signals) and the ionospheric delay experienced by a user on L5/E5a is about 1.8 times larger than on L1/E1.

3. Dual Frequency Monitoring Concept for Ionospheric Gradients

While it is possible to eliminate the ionospheric gradient threat using a dual frequency combination of GNSS signals, it might not be beneficial due to the significant increase in noise in the position solution and the required bounding of the residual errors in the protection level [8, 13]. A likely scenario for future service types is that positioning may still be based on single frequency methods, while a dual frequency mode is only used in case a GBAS ionospheric monitors triggers.

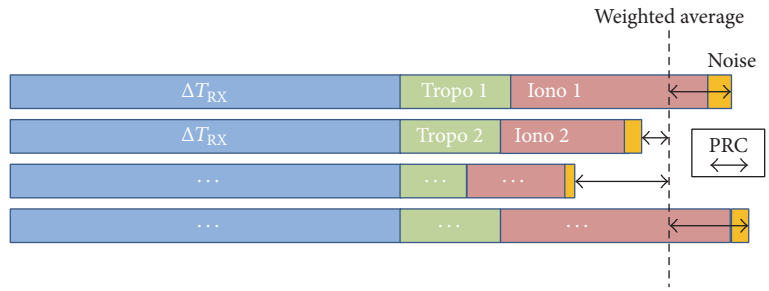

Figure 1: Illustration of the receiver clock adjustment process in the generation of pseudorange corrections (PRC).

In that case, however, mitigation of the ionospheric gradient threat is mandatory. Assuming that the ground station provides corrections for two frequencies and the aircraft receiver is also able to track signals on two frequencies, an effective ionospheric monitoring is possible. The proposed method marks a fundamental change where the monitoring is to be performed. While in GAST C it is the sole responsibility of the ground station to bound the errors at the airborne receiver, in GAST D the ionospheric monitoring task is shared between ground and airborne GBAS subsystems. In the method proposed here, it is the sole responsibility of the airborne systems to monitor ionospheric gradients. This allows for a more realistic error bounding because the current navigation performance (and aircraft performance) can be exploited and thus require less conservative assumptions.

The basic idea of the proposed monitoring is to simply compare the ionospheric delay estimate at the ground station with an ionospheric delay estimate at the aircraft. In the airborne system, it is possible to directly estimate the ionospheric delay $\widetilde{I}_{\mathrm{air},i}$ experienced on $\widehat{\rho}_{\mathrm{L1},i}$ based on the smoothed pseudorange measurements $\widehat{\rho}_{f,i}$ on frequency f and satellite i as

$$\widetilde{I}_{\mathrm{air},i} = \frac{f_{\mathrm{L5}}^2}{f_{\mathrm{L1}}^2 - f_{\mathrm{L5}}^2}\left(\widehat{\rho}_{\mathrm{L5},i} - \widehat{\rho}_{\mathrm{L1},i}\right). \tag{4}$$

As previously described, however, the ionospheric delay experienced at the ground station cannot be directly computed from the received corrections. Nevertheless, a pseudo-ionospheric delay estimate $\widetilde{I}_{\mathrm{PRC},i}$ for each satellite i can be formed from the GBAS corrections in the same way as when estimating the actual ionospheric delay on the L1 frequency from pseudorange measurements. The measured pseudorange is simply replaced with the received corrections from the ground station:

$$\begin{aligned}\widetilde{I}_{\mathrm{PRC},i} = \frac{f_{\mathrm{L5}}^2}{f_{\mathrm{L1}}^2 - f_{\mathrm{L5}}^2} \cdot \left[\left(\mathrm{PRC}_{\mathrm{L5},i} + \Delta t \cdot \mathrm{RRC}_{\mathrm{L5},i}\right)\right. \\ \left. - \left(\mathrm{PRC}_{\mathrm{L1},i} + \Delta t \cdot \mathrm{RRC}_{\mathrm{L1},i}\right)\right].\end{aligned} \tag{5}$$

In the same way as the applied correction would contain the pseudorange correction PRC and the range rate correction RRC multiplied with the time difference between the current time of measurement and the time of generation of the corrections Δt, these quantities are used also in the monitor. The indices L1 and L5 indicate the frequency for which the corrections were formed and f refers to the central frequency of the respective signals.

In a next step, these two quantities have to be made comparable. In order to do this, we remove the average of all N airborne ionospheric delay estimates per constellation to obtain a pseudo-airborne ionospheric delay measure $I_{\mathrm{air},i}$, given by

$$I_{\mathrm{air},i} = \widetilde{I}_{\mathrm{air},i} - \frac{1}{N}\sum_{i=1}^{N}\widetilde{I}_{\mathrm{air},i}. \tag{6}$$

In order to account for the fact that the airborne system may use only a subset of the satellites to which the ground system provides corrections, we repeat this process also with the pseudo-delay estimates from the ground station using only the set of satellites used in the airborne pseudo-ionospheric delay estimate. Similar to (6) the pseudo-ionospheric delay from the corrections is then

$$I_{\mathrm{PRC},i} = \widetilde{I}_{\mathrm{PRC},i} - \frac{1}{N}\sum_{i=1}^{N}\widetilde{I}_{\mathrm{PRC},i}. \tag{7}$$

These two estimates are now comparable and can be used to form a test statistic $I_{\mathrm{test},i}$ as

$$I_{\mathrm{test},i} = \left|I_{\mathrm{air},i} + I_{\mathrm{PRC},i}\right|. \tag{8}$$

This test statistic is then going to be compared with a monitoring threshold that is derived in the next section. Note that the two quantities are added (a more intuitive guess would be to subtract them and compare to zero) due to the fact that the pseudo-delay estimate from the corrections would have opposite sign of the value derived from the pseudorange measurements. In the nominal case (i.e., without a significant ionospheric gradient) the test statistic is small and would mostly consist of noise. With increasing decorrelation of the ionospheric delay experienced at the ground station and the airborne user, this quantity would increase.

The previously described test statistic is only valid if the navigation is based on signals in the L1/E1 frequency band. It is, however, also possible to support positioning based on L5/E5a which may, under certain circumstances, be a desired mode. In that case, a user would experience an ionospheric delay on each measurement that is $\beta = f_{\mathrm{L1}}^2/f_{\mathrm{L5}}^2 \approx 1.8$ times larger than on L1/E1. Additionally, the monitoring threshold

will be even tighter in that case. Thus, navigating based on L5/E5a is significantly more challenging in terms of integrity and is not considered further in this study.

4. Monitoring Threshold

After defining the test statistic above, a threshold needs to be determined, for when it is unsafe to use the signals from a certain satellite or set of satellites. A meaningful derivation of this monitoring threshold comes from the operation, namely, the requirements for a safe landing [14]. For a landing to be considered safe, the aircraft has to touch down inside the so-called "touchdown box," that is, not less than 200 ft and not more than 2700 ft behind the runway threshold and not less than 5 ft from either runway edge with a probability of not less than $1–10^{-6}$ in the nominal case [15, 16]. Two more cases are defined that also have to be considered, namely, the limit and the malfunction case. In the limit case, one parameter is kept at its most adverse value while all other influencing parameters vary according to their nominal distributions. In the malfunction case, an undetected error occurs. In both cases, the aircraft has to land within the touchdown box, where the land long limit is extended to 3000 ft behind the runway threshold.

These requirements are defined at aircraft level and thus only part of the total error budget can be attributed to the navigation system. The other main question in automatic landings, apart from how well the navigation system can determine the position of the aircraft, is how well the autopilot can land the aircraft on a desired spot. As the landing performance depends on both systems there is a possibility of trading off autopilot and navigation system performance. Note that this tradeoff is, however, only possible if the monitoring for disturbances occurs onboard the aircraft. In the case of the current service types, the ground station plays an important role in mitigating part of the threat space. Thus, it is not possible to take actual aircraft performance into account in those systems as the ground station has to support all aircraft types.

In [20], we showed the derivation of the monitoring threshold in the case a single satellite is affected by an ionospheric gradient. This was done by starting from the requirement that the aircraft has to land within the touchdown box and the land short case (i.e., landing not too close to the runway threshold) is considered to be the driving constraint. The along track error is a function of the nominal touchdown point NTDP, the nominal flight technical error FTE (i.e., how well the autopilot can place the aircraft onto the desired landing spot), the nominal navigation system error NSE (i.e., nominal errors due to noise, multipath, nominal ionosphere, and troposphere decorrelation), and an additional undetected error in form of a bias (e.g., caused by an ionospheric gradient). It is assumed that a vertical position error E_v maps into an along track position error E_{atrk} at touchdown by the simple geometric relation

$$E_{\text{atrk}} = \frac{E_v}{\tan(\text{GPA})}, \tag{9}$$

where GPA is the glide path angle (typically 3°). In the malfunction case, the aircraft has to land in the touchdown box with complete certainty. Taking the nominal NSE and FTE as Gaussian distributed random variables could of course never satisfy this condition. In that case, they are fixed at their 95th percentiles [17]. The requirement for the land short case can now be formulated as

$$200\,\text{ft} \leq \text{NTDP} - \frac{\text{NSE}_{\text{vert,ff,95\%}} + E_{v,\text{iono}}}{\tan(\text{GPA})} - \text{FTE}_{\text{ff,95\%}}, \tag{10}$$

where $\text{NSE}_{\text{vert,ff,95\%}}$ and $\text{FTE}_{\text{ff,95\%}}$ are the nominal navigation and flight technical errors at the 95th percentile of their Gaussian distributions. This is illustrated in Figure 2.

$\text{NSE}_{\text{vert,ff,95\%}}$ is a vertical position error and can be derived from the protection level equation [18] as

$$\sigma_{\text{NSE,vert,ff}} = \frac{\text{VPL}}{K_{\text{ffmd}}} = \frac{\text{VPL}}{5.81}, \tag{11}$$

where K_{ffmd} is the fault-free missed detection multiplier for the integrity risk of $2 \cdot 10^{-7}$ allocated to the protection level. Note that the VPL is a bound for the instantaneous nominal vertical position error and depends on both, the satellite geometry and the expected satellite ranging performance. At all times it must remain below the so-called vertical alert limit (VAL) that is limited by a value of 10 m for the final approach and landing.

The nominal touchdown point is usually considered to be located 1290 ft behind the runway threshold and $\sigma_{\text{FTE}} = 180\,\text{ft}$ is assumed to be a conservative value for all aircraft using GBAS [19]. With all those assumptions it is now possible to derive a limit on the largest vertical position error $E_{v,\text{iono}}$ due to an ionospheric anomaly using (10). Assuming $\text{VPL} = \text{VAL} = 10\,\text{m}$ and $\text{GPA} = 3°$, the resulting condition would be $E_v \leq 8.4\,\text{m}$. Taking a less conservative value of $\text{VPL} = 5\,\text{m}$ and leaving all other parameters constant, the resulting condition would already be relaxed to $E_v \leq 10.1\,\text{m}$. In the multiconstellation case $\text{VPL} = 2.5\,\text{m}$ is realistic and would further relax the required monitoring to $E_v \leq 10.9\,\text{m}$.

Given the test statistic per satellite described in (8), this limit in the position domain needs to be translated into a limit in the pseudorange domain. The pseudorange measurements ρ and the user position and clock estimate x are related by the weighted pseudoinverse S of the geometry matrix G. This matrix contains the normalized line-of-sight vectors between user and satellite in its rows and a vector of "1" in the fourth column for the user clock offset such that

$$x = S \cdot \rho. \tag{12}$$

A weighting matrix W containing the fault-free variances of the expected residual pseudorange errors is used to give lower weight to satellites with larger expected uncertainties. The S-matrix is defined as

$$S = \left(G^T W G\right)^{-1} G^T W \tag{13}$$

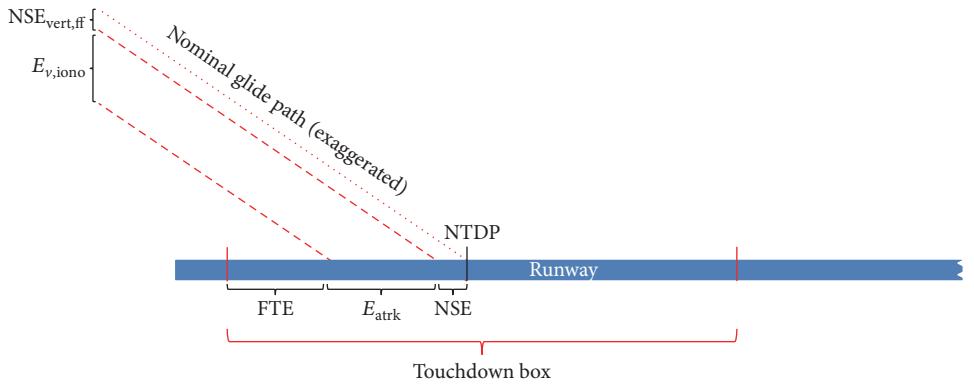

FIGURE 2: Derivation of the largest allowable vertical error $E_{v,\text{iono}}$ and illustration of the contributing error sources for automatic landings.

and the contribution of a single satellite i to the position estimate vertical to the approach track is given by

$$s_{\text{vert},i} = s_{3,i} + s_{1,i} \cdot \tan(\text{GPA}), \tag{14}$$

where $s_{k,i}$ denotes the entry in the kth row and ith column of the S-matrix.

In the case of a single satellite affected by an undetected ionospheric gradient, a limit on the pseudorange error $E_{r,\text{iono},i}$ for that particular satellite would be

$$E_{r,\text{iono},i} \leq \frac{E_{v,\text{iono}}}{|s_{\text{vert},i}|}. \tag{15}$$

It is interesting to note that, based on this equation, a pseudorange error may become arbitrarily large as long as the weight assigned to that satellite through $s_{\text{vert},i}$ is sufficiently small. A typical behavior of values for $s_{\text{vert},i}$ as a function of the elevation of the satellite is shown in Figure 3. Here the geometry of a combined GPS and Galileo constellation was simulated with 31 and 27 satellites, respectively, during our test flight described later in Section 5. At about 45° elevation s_{vert} of two satellites become almost zero, leading to very large pseudorange error limits.

With a missed detection probability of 10^{-9} attributed to the monitor and assuming that the noise in the test statistic follows a Gaussian distribution the monitoring condition is given as

$$I_{\text{test},i} \leq \frac{E_{v,\text{iono}}}{|s_{\text{vert},i}|} - 6.1 \cdot \sigma_{\text{monitor},i}. \tag{16}$$

The test statistic $I_{\text{test},i}$, as defined in (8), contains the airborne measurement noise $\sigma_{\text{air},f}$ from the smoothed pseudorange measurements on both frequencies f, as well as the pseudorange correction noise $\sigma_{\text{gnd},f}$ for both frequencies. The noise in the proposed monitor can thus be described as

$$\sigma_{\text{monitor},i} = \frac{f_{\text{L5}}^2}{f_{\text{L1}}^2 - f_{\text{L5}}^2} \sqrt{\sigma_{\text{gnd,L1}}^2 + \sigma_{\text{gnd,L5}}^2 + \sigma_{\text{air,L1}}^2 + \sigma_{\text{air,L5}}^2}. \tag{17}$$

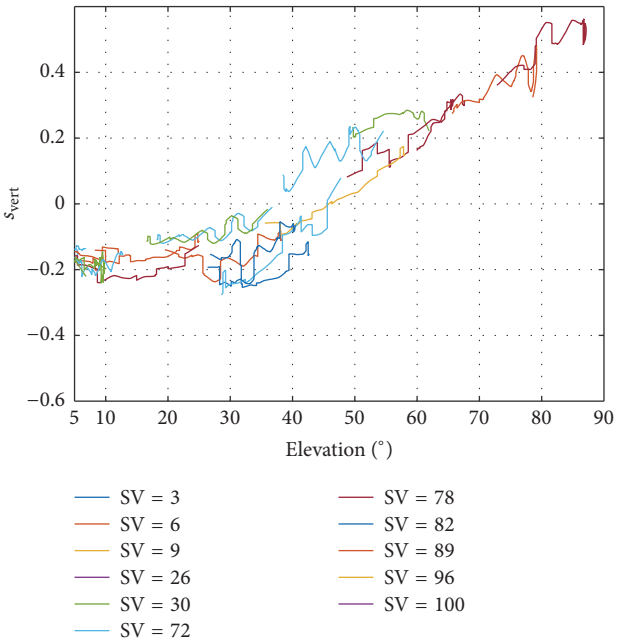

FIGURE 3: s_{vert} as a function of the elevation of the satellites for a future combined GPS (SVs 1–32)/Galileo (SVs 71–100) constellation with 31 and 27 satellites, respectively.

In [20] we showed that this monitoring condition can be fulfilled rather easily. Even with the minimum number of 5 satellites and noise from our experimental system (that is expected to be larger than that of an operational GBAS), the monitoring was possible and did not cause false alarms due to very low monitoring thresholds.

Unfortunately, assuming only a single affected satellite may not be sufficient to bound potential errors caused by ionospheric disturbances. It is possible that more than one satellite could be affected by an ionospheric front. For that reason, a scenario with two simultaneously affected satellites is investigated. In this case, the error from both affected satellites would project from the pseudorange into the position domain according to (12). A limit on the sum of both

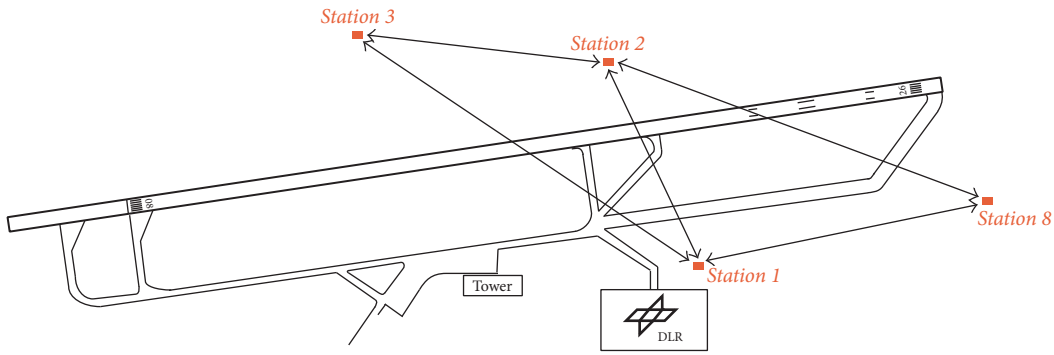

Figure 4: Layout of the GBAS reference stations at Braunschweig Airport as used during the flight trials.

pseudorange errors for the affected satellites i and k, using (15), then becomes

$$E_{r,\text{iono},i} + E_{r,\text{iono},k} \leq \frac{E_{v,\text{iono}}}{\left|s_{\text{vert},i} + s_{\text{vert},k}\right|}. \tag{18}$$

Finally, also the noise of both estimates needs to be considered and the monitoring condition becomes more stringent:

$$I_{\text{test},i} + I_{\text{test},k} \leq \frac{E_{v,\text{iono}}}{\left|s_{\text{vert},i} + s_{\text{vert},k}\right|} - 6.1 \cdot \sqrt{\sigma^2_{\text{monitor},i} + \sigma^2_{\text{monitor},k}}. \tag{19}$$

Note that, in this case, the test statistic can increase if the pseudo-ionospheric estimates on the two satellites have the same sign. At the same time, the noise contribution in the monitoring condition increases. The sum of s_{vert} can either increase or decrease depending on the sign of the values as shown previously in Figure 3. The worst case would occur when the satellites with the two largest s_{vert} and the same sign also have pseudo-ionospheric delays with the same sign that add up constructively.

This monitoring concept can of course also be expanded to consider more affected satellites. A generalized monitoring condition for N affected satellites would then be

$$\sum_{i=1}^{N} I_{\text{test},i} \leq \frac{E_{v,\text{iono}}}{\left|\sum_{i=1}^{N} s_{\text{vert},i}\right|} - 6.1 \cdot \sqrt{\sum_{i=1}^{N} \sigma^2_{\text{monitor},i}}. \tag{20}$$

Note that as more affected satellites are considered, the monitoring becomes more challenging. However, considering the cases with more affected satellites that are not excluded by other monitors becomes less likely with increasing N. Equation (20) does not take into account the low probability of occurrence but this can be included in the future if necessary. Furthermore, the monitoring is conservative in the way that it does not consider the actual separation of satellites in terms of azimuth angle. In the case of an ionospheric front, only satellites in certain azimuth regions would be affected; however, we consider only the s_{vert} values, irrespective of the azimuth.

The following section presents an exemplary evaluation during one of our flight trials. The contributing factors are analyzed more in detail with the example at hand to illustrate the effects inherent to this monitoring scheme.

5. Evaluation in Flight Trials and Discussion of the Monitor

The German Aerospace Center (DLR) is operating an experimental GBAS station consisting of four reference receivers tracking GPS and Galileo L1/E1 and L5/E5a signals. It is located at the Braunschweig research airport in northern Germany. The layout of the reference receiver locations is shown in Figure 4.

In November 2016 a flight test with a Dornier DO-228 aircraft (a twin-engine turboprop aircraft) was performed in the vicinity of Braunschweig. The flight lasted for about two hours and consisted of about one hour of maneuvering and flying the aircraft at different bank angles, followed by one hour of five approaches and extended traffic patterns. The ground track of the flight is shown in Figure 5. One of the purposes of the test was to evaluate the signal tracking performance in steep turns with bank angles of up to 60°. The data of that part of the flights shows frequent loss of lock events and very limited continuously tracked signals due to the banking of the aircraft [21]. That first part (shown in black in Figure 5) is therefore omitted in the following evaluations. Only the second half of the flight where normal maneuvering was performed (shown in green) is used.

Figure 6 shows a skyplot of the GPS Block IIF and Galileo satellites as observed during the test flight. There were 11 different satellites visible, at most 10 of them at the same time. This number is somewhat typical for a single full constellation. With a fully deployed Galileo constellation and all GPS satellites providing also L5 signals in the future, the number of visible satellites in Braunschweig would vary between 18 and 21.

We start the evaluations with assumptions on σ_{air} and σ_{gnd} which were experimentally derived from our ground and airborne systems for each of the two frequencies and each of the two constellations individually as previously presented in [8, 13]. For the whole flight and all satellites in the single affected satellite case, the test statistic (the monitoring condition for $i = 1$ in (20)) remains below the threshold, except one short instance that will be discussed later.

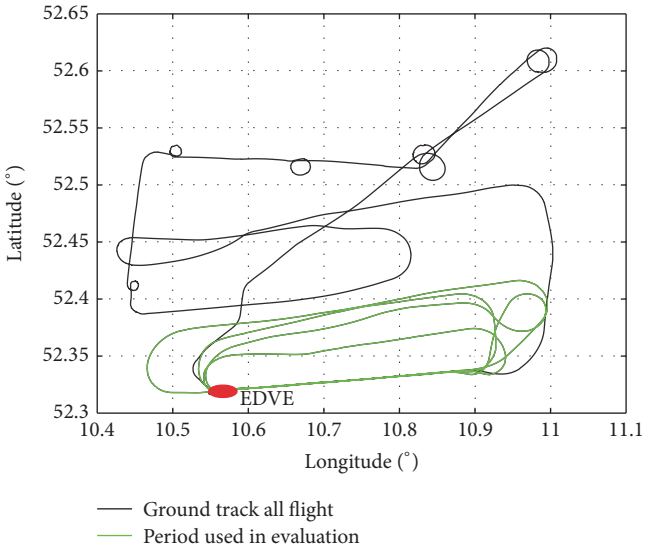

Figure 5: Ground track of the test flight around Braunschweig (ICAO identifier EDVE). The part used for the evaluation is shown in green.

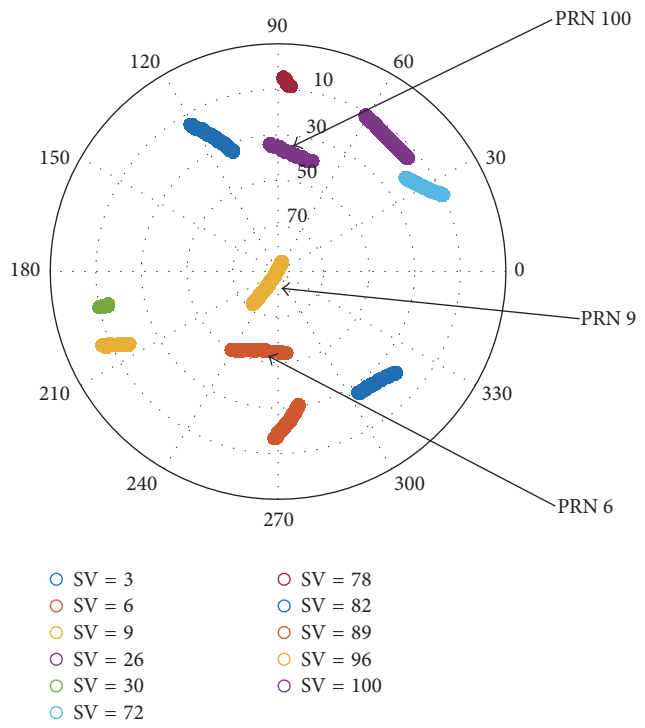

Figure 6: Skyplot of the combined GPS (SVs 1–32)/Galileo (SVs 71–100) constellation providing L1/E1 and L5/E5a signals as observed during the flight trial.

Figure 7 shows the number of used satellites in subplot (a) and the test statistics with the corresponding monitoring thresholds for L1/E1-based navigation for the three selected satellites marked in the skyplot in Figure 6. The drops in the number of satellites occur during turns where tracking of low elevation satellites is lost due to signal blockage by parts of the aircraft. Subplot (b) shows the results for PRN 6, a satellite at elevations between 50° and 55°. In the particular geometry, this satellite had a very small s_{vert} leading to an extremely large monitoring threshold mostly in the range of 100 m to 200 m (note the different scale of the y-axis for this subplot). As the satellite plays almost no role in the determination of the vertical position a potential error could become very large and not affect the user much. The threshold decreases to a value of about 3.7 m shortly before 16 h at the short period of time when the number of used satellites went down to 7. At that moment PRN 6 became a rather important satellite leading to a small threshold. The sharp drop in the monitoring threshold for all satellites at that time indicates a rather strong dependence on the number of satellites available in case that number is small. If many satellites are available, losing one or two of them for the position solution does not have a large impact anymore. Shortly before 15.8 h and at 16 h there are small spikes in the test statistic. They appear small due to the large scale of the y-axis but reach values of up to 7 m. These spikes result from excessive multipath or a cycle slip and were detected by the onboard GBAS monitor. However, for illustration purposes, we did not exclude the data from the plot. Due to the average removal in the test statistic as described in (6) an effect on one satellite would be visible in the test statistic of all other satellites as well.

This is the case as can be seen in subplot (c) showing the results for PRN 9 where spikes occur at the same times. PRN 9 is a very high elevation satellite between 72° and almost 90° elevation. At all times it is the satellite with the highest elevation. From a geometrical perspective, PRN 9 is a very important satellite and thus has a rather large s_{vert}. According to (15) this results in a small tolerable pseudorange error for that satellite and thus a low monitoring threshold throughout the flight. Due to the average removal in forming the test statistic the threshold for that satellite is exceeded twice just before 16 h; however, that effect by a cycle slip would have been excluded by other monitors and is again in the data just for illustration purposes.

The results for PRN 100, a Galileo satellite, are shown in subplot (d). Note that the average removal is performed per constellation and thus the spikes from subplots (b) and (c) do not occur in subplot (d). The elevation of the satellite varies between 35° and 40°. While it has quite a large weight in the beginning, it quickly becomes smaller and thus the monitoring threshold increases fast to larger values.

Figure 7 showed exemplary results for the monitoring condition for a single affected satellite. The case of more than one affected satellite will probably have to be considered for monitoring as well. We therefore also considered the case of two affected satellites; that is, $i = 2$ in (20).

Figure 8 shows the minimum over all thresholds for all possible subsets of two affected satellites during the flight test in red, together with the test statistic in black. The solid lines of the monitoring thresholds are using our own experimentally derived characterization of noise in the corrections and airborne measurements, while the dashed lines assume the performance that can be expected from an operational GBAS station with multipath limiting antennas in carefully protected sites and from airborne equipment with a reasonably

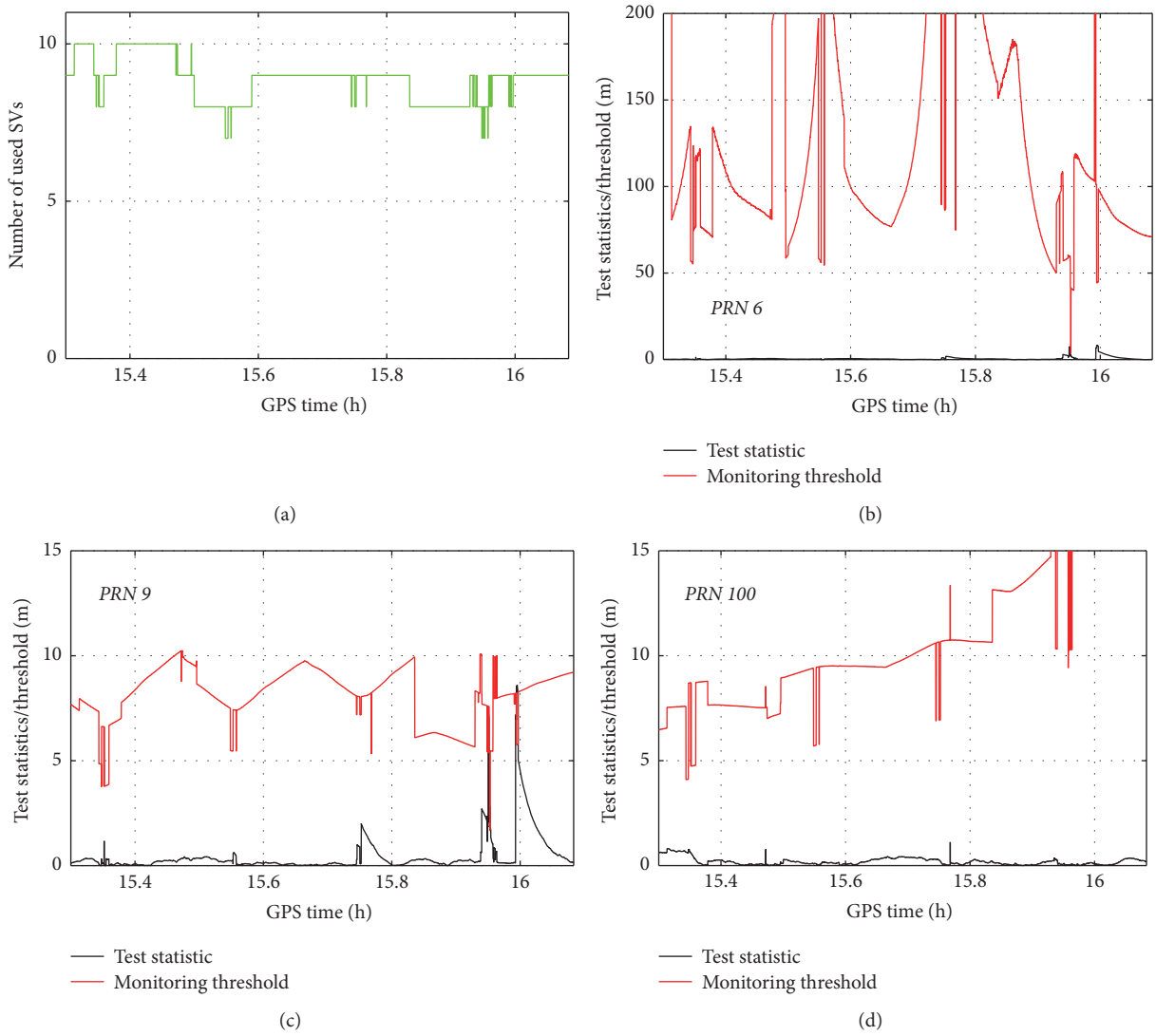

FIGURE 7: Test statistic and monitoring threshold for three example satellites.

good airborne antenna performance as presented in [9, 18]. These models can be considered realistic, while the performance of our own equipment is slightly worse and thus yields conservative results. It can be noted again that the monitoring threshold has sharp drops whenever we lose satellites in turns. At about 15.35 h and 15.95 h the monitoring threshold even becomes negative and thus, of course, makes the monitoring completely impossible assuming our own noise models. The black curve is the corresponding test statistic that is regularly exceeding the threshold whenever a drop in the number of used satellites and thus in the monitoring threshold occurs. However, recall that the experimental thresholds in red were derived from the actual measurements during the flight with a maximum of 10 satellites. Looking into the future and simulating complete dual frequency GPS and Galileo constellations with 31 and 27 satellites, respectively, the situation looks very much different. This is shown in the same plot in green. The monitoring threshold now reaches a minimum of 7.8 m at about 15.75 h. With two full dual frequency capable constellations, the monitoring thresholds will be large enough to provide sufficient margin to prevent false alarms due to noise effects for the case of two affected satellites.

This concept can be further extended to three and four affected satellites. This, of course, places a greater burden on the monitoring and yields again decreasing monitoring thresholds. Figure 9 shows simulated monitoring thresholds for the aircraft positions during the test flight assuming two, three, and four affected satellites in black, red, and green, respectively. As expected, the monitoring threshold keeps decreasing while more satellites are assumed to be affected.

But even in the case of four affected satellites the threshold just reaches values of around 4 m and thus remains above the threshold for two affected satellites and for the limited constellation we observed during the flight test.

Now the results so far only showed an example of a short time period in mid-latitudes with a rather good satellite geometry. For that reason, we also examined the effect of the satellite geometry in less favorable locations and chose as an

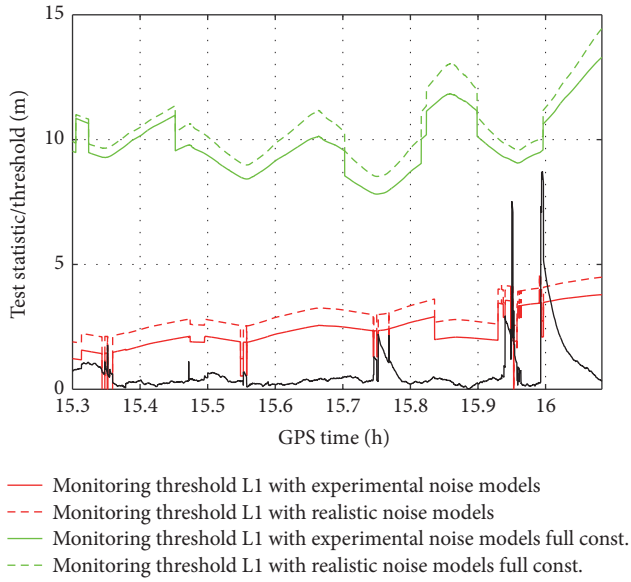

Figure 8: Monitoring thresholds for the case of two affected satellites with the constellation as seen during the flight trials (red) and simulated full GPS + Galileo constellation (green).

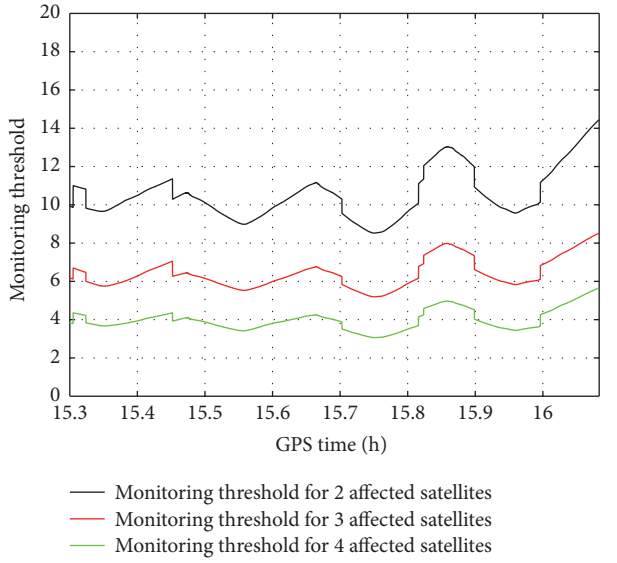

Figure 9: Monitoring thresholds assuming two full dual frequency capable constellations and 2, 3, and 4 simultaneously affected satellites.

example Troll Research Station in Antarctica located at 72° southern latitude. The results are shown in Figure 10. Due to the lack of high elevation satellites, the geometries become weaker in the vertical domain and thus lead to somewhat larger s_{vert} values. However, the monitoring for the 2 and 3 affected satellite cases still seems to be possible, for the 4 affected cases there are times, for example, around midnight, where the threshold is rather small. At all times the threshold remains positive and thus makes the monitoring possible in principle depending on the assumed noise in the measurement.

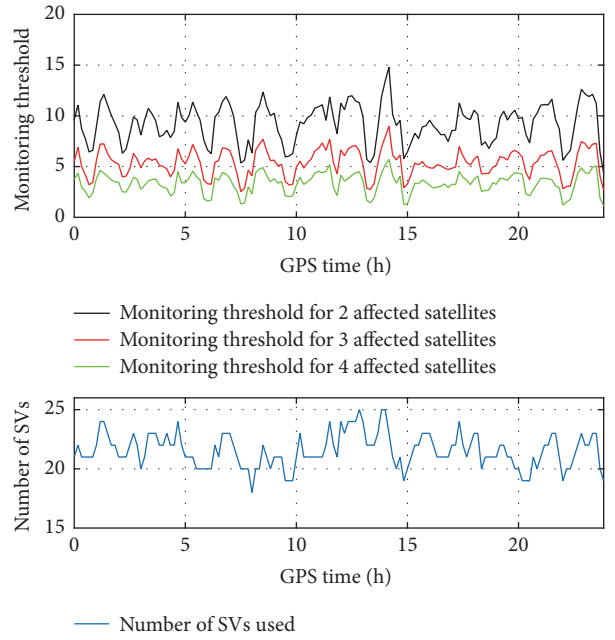

Figure 10: Monitoring threshold for Troll (Antarctica at 72° Southern Latitude) as example for a location with less favorable satellite geometry and the effect on the monitoring.

6. Discussion and Conclusions

In this paper, we presented a possibility for using dual frequency corrections and airborne measurements to monitor ionospheric gradients between a GBAS ground station and an airborne user. We showed the definition and calculation of a test statistic based on pseudo-ionospheric delay estimates. In a next step, we derived a monitoring threshold from autoland requirements for the case of one or more satellites that are potentially affected by an ionospheric gradient. Then we used flight test data where we had up to 10 dual frequency satellites of the latest generation of GPS and Galileo available to evaluate the performance of the monitor experimentally. The main findings showed that the monitoring is feasible in principle. By design, the monitor is sensitive to the satellite geometry at a given time. Thus, loss of lock of satellites decreases the monitoring performance. However, the tests were carried out in a scenario with a limited number of satellites. Assuming two full dual frequency constellations greatly simplifies the monitoring task and will enable safe and reliable monitoring in the case of single frequency positioning using dual frequency monitoring which is one of the likely scenarios for a future GBAS service.

The proposed monitoring follows a new philosophy where the monitoring for ionospheric gradients should occur. In the currently operational service type C ionospheric threat mitigation is the responsibility of the ground station. In the service type D, the responsibility is shared between the ground and the airborne system. Both, however, rely on conservative assumptions and the validity of ionospheric threat models. Moving the monitoring to the airborne system as proposed in this paper is a lot less conservative since the monitoring threshold is derived based on the satellite geometry

used by the airborne receiver and thus reflecting much better the current positioning performance. It furthermore provides the possibility for airframe integrators to also use realistic models for the autopilot performance (in terms of σ_{FTE}) and thus obtain even larger monitoring thresholds. At all times the monitor achieves the same level of safety and relaxes the monitoring requirement only by replacing conservative assumptions with more realistic information that is available in the aircraft.

Conflicts of Interest

The authors declare that there are no conflicts of interest regarding the publication of this paper.

References

[1] Working Group C, "ARAIM Technical Subgroup—Milestone III Report," February 2016, http://ec.europa.eu/growth/tools-databases/newsroom/cf/itemdetail.cfm?item_id=8690.

[2] T. Dautermann, "Civil air navigation using GNSS enhanced by wide area satellite based augmentation systems," *Progress in Aerospace Sciences*, vol. 67, pp. 51–62, 2014.

[3] T. Fujiwara and T. Tsujii, "GBAS availability assessment and modelling of ionospheric scintillation effects," in *Proceedings of the ION's Pacific PNT Meeting*, Honolulu, Hawaii, USA, April 2015.

[4] M. Yoon, D. Kim, J. Lee, and S. Pullen, "Multi-dimensional verification methodology of ionospheric gradient observations during plasma bubble events in the Brazilian Region," in *Proceedings of the ION's Pacific PNT Meeting*, Honolulu, Hawaii, USA, April 2015.

[5] N. Hlubek, J. Berdermann, V. Wilken et al., "Scintillations of the GPS, GLONASS, and Galileo signals at equatorial latitude," *Journal of Space Weather and Space Climate*, vol. 4, article A22, pp. 1–7, 2014.

[6] S. Jung and J. Lee, "Long-term ionospheric anomaly monitoring for ground based augmentation systems," *Radio Science*, vol. 47, no. 4, Article ID RS4006, 2012.

[7] M. Kim, Y. Choi, H.-S. Jun, and J. Lee, "GBAS ionospheric threat model assessment for category I operation in the Korean region," *GPS Solutions*, vol. 19, no. 3, pp. 443–456, 2015.

[8] M.-S. Circiu, M. Felux, B. Belabbas et al., "Evaluation of GPS L5, Galileo E1 and Galileo E5a performance in flight trials for multi frequency multi constellation GBAS," in *Proceedings of the ION GNSS*, Tampa, Fla, USA, 2015.

[9] ED-114A, "Minimum operational performance specification for global navigation satellite ground based augmentation system ground equipment to support category I operations," EUROCAE, 2013.

[10] R. Hatch, "The synergism of GPS code and carrier measurements," in *Proceedings of the International Geodetic Symposium on Satellite Doppler Positioning*, vol. 1, 1983.

[11] M. Stanisak, A. Lipp, and T. Feuerle, "Possible VDB formatting for multi-constellation / multi-frequency GBAS services," in *Proceedings of the 28th International Technical Meeting of the Satellite Division of the Institute of Navigation (ION GNSS '15)*, pp. 1507–1518, Tampa, Fla, USA, September 2015.

[12] C. Milner, A. Guilbert, and C. Macabiau, "Evolution of corrections processing for the MC/MF Ground Based Augmentation System (GBAS)," in *Proceedings of the International Technical Meeting ION (GNSS '15)*, Dana Point, Calif, USA, 2015.

[13] D. Gerbeth, M.-S. Circiu, M. Caamano, and M. Felux, "Nominal performance of future dual frequency dual constellation GBAS," *International Journal of Aerospace Engineering*, vol. 2016, Article ID 6835282, 20 pages, 2016.

[14] W. Schuster and W. Ochieng, "Harmonisation of category-III precision approach navigation system performance requirements," *Journal of Navigation*, vol. 63, no. 4, pp. 569–589, 2010.

[15] AC 120-28D, "Criteria for approval of category III weather minima for takeoff, landing, and rollout," FAA, 1999.

[16] CS-AWO, "Certification Specifications for All Weather Operations," EASA, 2003.

[17] B. Clark and B. DeCleene, "Alert limits: do we need them for CAT III? Deriving GBAS requirements for consistency with cat III operations," in *Proceedings of the Institute of Navigation—19th International Technical Meeting of the Satellite Division (ION GNSS '06)*, pp. 3070–3081, Fort Worth, Tex, USA, September 2006.

[18] DO-253C, "Minimum operational performance standards for GPS local area augmentation system airborne equipment," RTCA, 2009.

[19] "Conceptual Framework for the Proposal for GBAS to Support CAT III Operations," in *Proceedings of the ICAO NSP 3 Meeting*, Montreal, Canada, December 2016.

[20] M. Felux, M.-S. Circiu, D. Gerbeth, and M. Caamano, "Experimental validation of an ionospheric monitoring scheme for dual frequency GBAS," in *Proceedings of the ION GNSS+*, Portland, Ore, USA, 2016.

[21] M. Rippl, I. Martini, B. Belabbas, and M. Meurer, "ARAIM operational performance tested in flight," in *Proceedings of the International Technical Meeting ION*, San Diego, Calif, USA, January 2014.